International Journal of Pharmaceutics 624 (2022) 122007

Contents lists available at ScienceDirect

International Journal of Pharmaceutics

journal homepage: www.elsevier.com/locate/ijpharm

# Lipid nano-vesicles for thyroid hormone encapsulation: A comparison between different fabrication technologies, drug loading, and an *in vitro* delivery to human tendon stem/progenitor cells in 2D and 3D culture

E.P. Lamparelli [a], M.C. Ciardulli [a], P. Scala [a], M. Scognamiglio [b], B. Charlier [a], P. Di Pietro [a], V. Izzo [a], C. Vecchione [a,c], N. Maffulli [a], G. Della Porta [a,b,d,*]

[a] Department of Medicine, Surgery and Dentistry, University of Salerno, Via S. Allende, 84081 Baronissi, (SA), Italy
[b] Department of Industrial Engineering, Università di Salerno, via Giovanni Paolo I, 84084 Fisciano, (SA), Italy
[c] IRCCS Neuromed, Department of Vascular Physiopathology, 86077 Pozzilli, IS, Italy
[d] Interdepartment Centre BIONAM, Università di Salerno, via Giovanni Paolo I, 84084 Fisciano, (SA), Italy

ARTICLE INFO

*Keywords:*
Nano-vesicles
Liposomes
Drug delivery
T3 hormone
Tendon progenitor stem cells

ABSTRACT

Phosphatidylcholine (PC) vesicles loaded with Triiodothyronine (T3) were fabricated using different manufacturing methods: thin layer hydration plus sonication (TF-UF), supercritical liposome formation (SC), and microfluidic technology (MF). Vesicles obtained by MF had the lowest mean diameter (88.61 ± 44.48 nm) with a Zeta Potential of −20.1 ± 5.90 mV and loading of 10 mg/g (encapsulation efficiency: 57%). In contrast, SC vesicles showed extremely low encapsulation efficiency (<10%) probably due to T3 solubility in ethanol/carbon dioxide mixture; despite TF-UF vesicles exhibiting good size (167.7 ± 90 nm; Zp −8.50 ± 0.60 mV) and loading (10 mg/g), poor mass recovery was obtained (50% loss). MF vesicles had low cytotoxicity, and they were well enough internalized by both HeLa and human tendon stem/progenitor cells (hTSPCs). Their biological activity was also monitored in both 2D and 3D cultures of hTSPCs supplemented with therapeutical concentrations of PC/T3 nano-liposomes. 2D culture showed almost similar constitutive gene expression compared to control culture supplemented with free-T3. On the contrary, when hTPSCs 3D culture was assembled, it showed a more evident homogeneous distribution of FITC labeled vesicles within the high-density structure and a significant upregulation of cell constitutive genes, such as type I Collagen (4.8-fold; $p < 0.0001$) at day 7, compared to the control, suggesting that T3/PC formulation has increased T3 cytosolic concentration, thus improving cells metabolic activity. The study supported MF technology for nano-carriers fabrication and opens perspectives on the activity of PC/T3 nano-vesicles as innovative formulations for TPSCs stimulation in ECM secretion.

## 1. Introduction

Liposomes are vesicular carriers, consisting of an aqueous core entrapped by one or more lipid bilayers, which form spontaneously starting from contact between an organic phase and water one (Chacko et al., 2020). Specifically, when certain phospholipids are hydrated in aqueous media generate closed structures, very stable in thermodynamic terms, which can be functionalized both with hydrophilic and hydrophobic drugs (Siontorou et al., 2017). These carriers are extremely biocompatible, being constituted by lipids mimicking the natural composition of biological membranes (Li et al., 2015). Hydrophilic drugs can be captured from the aqueous core, while hydrophobic ones by the lipid bilayer; this last one can also contain other constituents for improving pharmacokinetic properties, making liposomes extremely versatile tools (Kashapov et al., 2021); (Arshinova et al., 2012; Samuni et al., 2000).

Liposomes, according to the number of bilayers, can be classified into two categories: unilamellar (ULV) and multilamellar vesicles (MLV). Unilamellar vesicles have a single phospholipid bilayer and can be classified, depending on size, into large (LUV) and small unilamellar vesicles (SUV) (Kim and Jeong, 2021). Conversely, multilamellar ones have two or more concentric bilayers and present larger sizes (Bozzuto

* Corresponding author at: Della Porta Giovanna, Department of Medicine, Surgery and Dentistry, University of Salerno, Via S. Allende, Baronissi, (SA) 84084, Italy.
*E-mail address:* gdellaporta@unisa.it (G. Della Porta).

https://doi.org/10.1016/j.ijpharm.2022.122007
Received 26 January 2022; Received in revised form 6 June 2022; Accepted 5 July 2022
Available online 9 July 2022

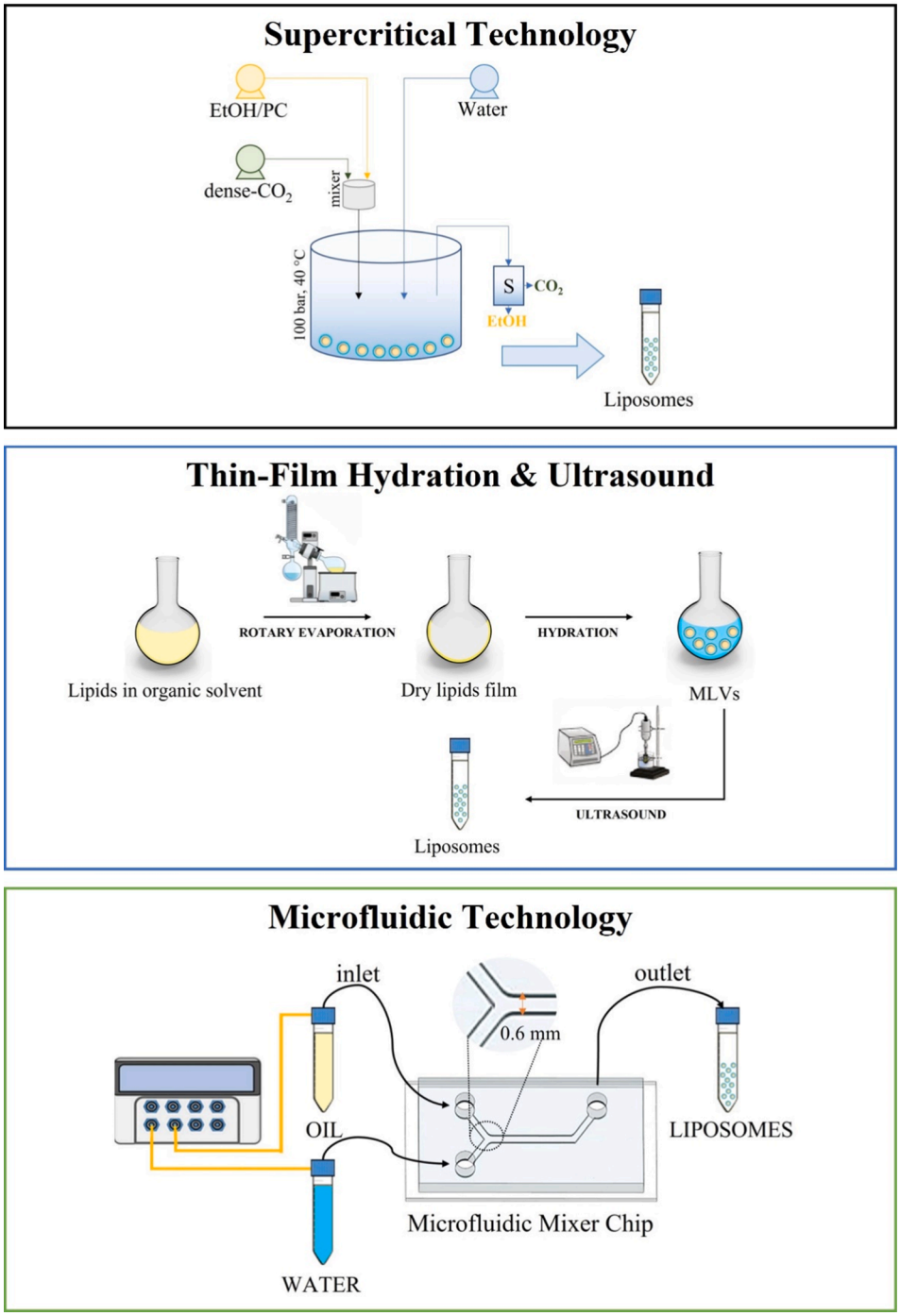


**Fig. 1.** Schematic description of different technologies tested.

and Molinari, 2015). Several post-production manipulations are often required to decrease vesicle sizes, such as extrusion or sonication because dimension and charge density are the most critical parameters for cellular uptake (Danaei et al., 2018)(Kohli et al., 2014). Furthermore, vesicle physical stability in suspension is also important to avoid aggregation processes that would change their particle size distribution (PSD) (Heurtault, 2003). Neutral liposomes do not interact significantly with cells owing to negative cellular membrane potential; therefore, the presence of a suitable electrostatic charge on the surface of vesicles is important to promote liposome-cell interaction (Liu et al., 2021). For this reason, cationic Liposomes (CL) seem to be very promising in gene therapy (Balazs and Godbey, 2011); indeed, they exhibit a high affinity to cell membranes and can deliver exogenous material intracellularly via fusion with them. The Positive surface charge may not only enhance the uptake by target cells but also accelerate their plasma clearance after systemic administration (Immordino et al., 2006) (Gabizon and Papahadjopoulos, 1988).

Drug delivery from liposomes can be due to temperature and/or pH variation (Zhao et al., 2020). Traditional thermosensitive liposomes are composed of lipids that underwent a gel-to-liquid phase transition at several degrees above physiological temperature. More recently, temperature-sensitization of liposomes has been demonstrated with the use of phospholipids and synthetic temperature-sensitive polymers. Polymer-modified liposomes, that achieve temperature response via temperature-dependent interactions between polymers and the lipid membrane, have been extensively studied (Ta and Porter, 2013);

whereas, pH-responsive liposomes can be employed to effect site-specific drug release. Since some pathological sites have different pH profiles from that of normal tissues, these pH changes can trigger changes in the permeability of the liposomal membrane by protonation/deprotonation of functional groups that induce morphological changes in the lipid bilayers (Lee and Thompson, 2017).

On the other hand, literature largely describes cellular internalization of these vesicles (Andar et al., 2014), showing that liposomes are predominantly endocytosed through either the clathrin- or caveolin-mediated endocytosis (Hong et al., 1985; Scherphof and Kamps, 1998; Straubinger et al., 1983). Therefore, in the case of liposome, it would be more adequate to indicate the specific drug targeting or delivery and not a proper drug release, as can be obtained in the case of different nano-carriers, such as biopolymers ones (Palazzo et al., 2021). Indeed, the principal use of liposomal carriers is more properly adopted when a biomolecule should be delivered into a specific cellular structure or tissue/organ.

Several technologies can be used to fabricate these vesicles from Thin-Film hydration procedure (Shah et al., 2020) to the recently described processes based on supercritical fluids (Campardelli et al., 2016; Espirito Santo et al., 2014, 2015) or microfluidic approaches (Yu et al., 2009). Furthermore, a huge amount of molecules and drugs with varying lipophilicity can be encapsulated in the phospholipid bilayer or the aqueous core as well as at the interface, like antineoplastic (Cosco et al., 2012; Fresta and Puglisi, 1996), antimicrobial drugs (Siler-marinkovic et al., 1997), steroids (Vermorken et al., 2011), anesthetic (Cipollaro et al., 2020), vaccines (such as the one largely discussed against SARS-CoV-2), and other genetic material (Miller, 2003; Simões et al., 2005). Drugs entrapped within liposomes are not immediately bioavailable, and are released by pH or thermal variations as well as directly delivered following the cellular uptake. In such case, they can be used to increase the cytosolic concentration of certain drugs, which are normally poorly taken up into cells.

It is well-known that thyroid hormones (THs), i.e. T3 (triiodothyronine) and T4 (thyroxine), play a key role in the development and metabolism of many tissues and organs. In particular, the effect of these hormones is mediated mainly through cytosolic activity of T3, which regulates gene expression by binding to the TH receptors (TRs)-a and -b. However, in contrast to progesterone (PR) and glucocorticoid receptors (GR), unliganded TR localizes primarily to the nucleus and interacts with nucleosome-embedded DNA. Unliganded, chromatin-bound TR represses transcription through direct interaction with transcriptional co-repressors such as SMRT and NCoR. The binding of hormone is thought to induce a conformational change of TR, causing displacement of co-repressors and recruitment of co-activators. This relatively simple bimodal switch results in a transition from gene repression to gene activation (Grøntved et al., 2015).

Recent studies have highlighted the presence of TRs in tendon tissue, assuming an involvement of THs in the proliferation and apoptosis of mature tenocytes. Further studies provided evidence of a significant association between thyroid hormones and tenocyte ECM proteins secretion, especially type I collagen (Berardi et al., 2014; Ciardulli et al., 2022; di Giacomo et al., 2017; Oliva et al., 2013).

Several authors described a successful encapsulation of T3 hormone within different vesicles to improve its cellular uptake; for instance, Fountain et al. (1982) reported its entrapment within MLV, composed of a mixture of Dimyristoylphosphatidylcholine (DMPC): Cholesterol (Cho1): Dicetylphosphate (DCP) in a molar ratio of 7:2:1 and with a loading around 60% (Fountain et al., 1982). Whereas, Pireddu et al. (2018) have proposed three different T3 vesicle systems, such as conventional, stealth (PEGylated), and Lactoferrin (Lf)-modified-Stealth liposomes, obtained by film hydration method with a loading around 90%. In this sense, the use of liposomal formulation should improve the T3 delivery and its accumulation within the cells to reach the cellular nucleus (Pireddu et al., 2018).

Following these indications, PhosphatidylCholine (PC) nano-vesicles loaded with Triiodothyronine (T3) were fabricated using three different technologies, and their size distributions, surface charge, morphology, and drug loading were compared. Vesicles cytotoxicity and related cellular uptake were also investigated by MTT assay and confocal microscopy, respectively, using both HeLa cell line and primary Tendon Stem/Progenitor Cells (TSPCs). In this last case, tendon surgery explants were firstly harvested from patients undergoing reconstruction of anterior cruciate ligaments to achieve *in vitro* primary cells culture (Bi et al., 2007; Huang et al., 2021). Uptake and biological activity of PC/T3-loaded were explored in TPSCs both 2D and 3D culture, by monitoring cell constitutive gene expressions such as type *I* and *III Collagen*, *Scleraxis-A*, *Decorin*, and *Tenascin-C* by Real Time-PCR after 7 and 14 days of treatment, respectively.

## 2. Materials & methods

### 2.1. PC vesicles preparation

Vesicles were prepared according to the Thin-Film hydration procedure followed by multiple Ultrasound and Filtration (TF-UF) steps (Bangham et al., 1965) using phosphatidylcholine and 3,3′,5-Triiodo-L-thyronine sodium salt (T3) (PC, Cat. No BCBS7601, Sigma Aldrich). A solution of 10 mg/mL of PC was first dissolved in chloroform to obtain a thin film, then, hydrated with 10 mL of phosphate-buffered saline (PBS); at this point, ultrasound cycles (n. 5) by a digital probe (Elmasonic P, Elma Schmidbauer GmbH, DE) operating at 30% of its amplitude for 30 sec were performed and the suspension was filtered with a 0.22 μm membrane (see Fig. 1).

Supercritical Assisted Liposome Formation (SC) protocol ensures the ethanol and water solutions mix by means of supercritical carbon dioxide (Ciaglia et al., 2019) (Trucillo et al., 2020). At first, PC (10 mg/mL) was dissolved into ethanol/carbon dioxide solution at pressure and temperature conditions of 10 MPa and 38 °C; then, this high-pressure mixture was added to a reactor where the water phase (ratio 1:3) was sprayed through a nozzle of 80 μm to continuously improve the two phases mixing. Ethanol was continuously extracted from water suspension and recovered in a separator by a depressurization step from 100 bar to 10 bar; whereas water plus vesicles suspension was continuously collected from the bottom of the high-pressure chamber, at PC concentration of 2 mg/mL (see Fig. 1).

Microfluidic technique (MF) was performed adopting the Nano-Generator Flex (Precigenome LLC San Jose, CA- USA) by injecting the lipid mixture (consisting of ethanol and PC at 5 mg/mL) and water within a Y-shaped microfluidic chip at constant Flow Rate Ratios (FRR) 1:3 (ethanol/water) and adapting the Total Flow Rate (TFR) to obtain a final PC concentration of 1 mg/mL.

### 2.2. Vesicle morphology, mean size, and surface charge

Vesicle morphology was observed by field emission-scanning electron microscopy (FE-SEM, mod. LEO 1525, Carl Zeiss SMT AG, Oberkochen, Germany). Several droplets were placed on a double-sided adhesive carbon tape previously stuck to an aluminum stub and dried by a critical point drier (mod. K850, Quorum Technologies Ltd, East Sussex, United Kingdom); then, coated with a thin gold film (layer thickness 250 Å) using a sputter coater (mod.108 A, Agar Scientific, Stansted, United Kingdom).

10 μl of each liposome suspension was applied onto the formvar/carbon 200 mesh copper grid (Ted Pella, USA Cat. No. 01800-F) and dried for several hours before imaging. Transmission electron microscope (TEM) micrographs in bright-field modes were taken by FEI TECNAI $G^2$ 200 kV S-TWIN microscope equipped with a 4 K camera (electron source with $LaB_6$ emitter; FEI Company, Dawson Creek Drive, Hillsboro, OR, USA). Bright-field (BF) TEM images were acquired at 120 kV using a spot size equal to 3, integration time 1 s.

Vesicle sizes, distributions, and Zeta potential were measured by the

dynamic light scattering (DLS) technique, using Nano ZS Malvern Zeta Sizer (model 1000HSa, UK) at 25 °C, equipped with a He-Ne laser of 633 nm and a detector angle of 173℃. Three independent measurements were performed for each sample just after preparation.

### 2.3. Loading and analytical methods for T3

3,3′,5-Triiodo-L-thyronine sodium salt (T3) (Cat. No BCBS7601, Sigma Aldrich) was analyzed with a Waters 1525 Model Binary HPLC chromatographic system equipped with a multiple wavelength fluorescence detector (Model 2475) and a refrigerated autosampler (Model 2707). Mobile phases, composed of 0.1 % trifluoroacetic acid (A) and 80% acetonitrile (B), were used for chromatographic separation; both solvents were HPLC grade, and the mobile phases were degassed in an ultrasonic bath sonicator (Elma, CT, USA) for 20 min prior to use. Total flow rate was set at 1.0 mL/min and a gradient elution was used as follows: 25% of solvent B for 1 min, followed by a linear gradient from 25 % to 85 % of solvent B over 3 min, a 1-minute step at 85% of solvent B and a final equilibration step at 25% B hold for 1.5 min. An XBridge column (XBridge $C_{18}$. 4.6 × 50 mm, 3.5 μm, Waters) was used for resolving analytical peaks. The autosampler temperature was maintained at 4 °C during analysis. The injection volume was 20 μl. Samples were detected at a wavelength of 225 nm. To build a calibration curve, pure T3 was dissolved in 1 M Ethanol/HCl at a 4:1 ratio, and added to a blank phospholipid matrix, previously dissolved in chloroform. Six concentration points (0, 0.5, 2.5, 5, 10, 20 μg/ml) were used, and a linear regression with a $R^2$ of 0.997 was obtained. Chromatographic data were analyzed with Breeze 2 software® (Waters).

Loading was calculated by analyzing the T3 content in the dried pellet previously weighted. Dried pellet was obtained by ultracentrifugation at 30,000 rpm for 4 h, followed by a speed vacuum drying. The drug loading was calculated following the Eq. (1):

$$\text{Loading} = \frac{AmountofT3detected(\mu g)}{Weightofsample(g)} \quad (1)$$

Encapsulation efficiency (EE, %) was calculated using the Eq. (2):

$$\text{EE}\,(\%) = \frac{AmountofT3detected}{AmountofT3loaded} \text{ x } 100 \quad (2)$$

### 2.4. Dilution integrity test

T3 stock solution was added to the extracted matrix to obtain a concentration equal to three times the highest point of the calibration curve and then diluted with other blank matrices at concentrations of 1/3, 1/5 and1/10 of the initial sample. Samples obtained with this procedure were extracted and analyzed according to the methodology described above. Precision and accuracy integrity of the QC dilution resulted within the limit of ± 15% of the nominal concentration for all analyzed points.

### 2.5. Analysis of solvents residual using GC/FID with headspace

Ethanol residue in the vesicles suspensions was analyzed to monitor the efficiency in ethanol removal, following the dialysis process (in the case of MF technology) or by dense gases (in the case of SC one). In more detail, the solvent residue was measured using a headspace sampler (mod. 7694E; Agilent Technologies Inc, Wilmington, Delaware) coupled to a Gas Chromatograph interfaced with a Flame Ionization Detector (GC-FID; mod. 6890 Agilent Series; Agilent Technologies Inc., Wilmington, Delaware). Ethanol was separated using a fused-silica Rtx®-Volatiles (proprietary Crossbond® diphenyl/dimethyl polysiloxane phase) capillary column of 30 m length, 0.53 mm internal diameter, 2 μm film thickness (mod. 10,902 Restek Corp., Bellefonte, PA). GC oven was programmed with an initial temperature of 40 °C for 5 min and then ramped at a temperature gradient of 7 °C/min to 150 °C. The helium was used as the carrier gas and its flow rate was set to 1 mL/min and each sample was injected into the column using the split mode (ratio 4:1) with the injection port temperature set at 200 °C. Specific headspace conditions were: equilibration time 25 min at 100 °C, pressurization time 2 min, and loop fill time 1 min. Headspace samples were prepared in 22 mL vials filled with 4 mL of suspension. Analyses were performed on each sample in three replicates.

### 2.6. Human Tendon Stem/Progenitor cells extraction and harvesting

The primary cell population included in the study was extracted from surgical samples obtained from patients recruited for the reconstruction of anterior cruciate ligaments. Samples were collected according to the guidelines of the Declaration of Helsinki approved by the Institutional Review of San Giovanni di Dio e Ruggi D'Aragona Hospital (Salerno, Italy). Review Board (prot./SCCE n. 151 achieved on 29 October 2020).

Tendon samples were washed with sterile PBS supplemented with 1% Penicillin/Streptomycin (Corning, Manassas, VA, United States) and 1% Amphotericin B (Corning, Manassas, VA, United States) and cut into small pieces to be digested with Trypsin-EDTA solution (Corning, Manassas, VA, United States) for 30 min at 37 °C. Further details are reported elsewhere (Ciardulli et al., 2022). Culture medium consisted of Dulbecco's modified Eagle's medium (D-MEM, Sigma-Aldrich, St. Louis, MO, USA) containing 10% fetal bovine serum and 1% penicillin/streptomycin solution. Two different explants were cultured and three subcultures for each explant were used for the experiments at passage 3.

### 2.7. Cytotoxicity studies

HeLa cell line was seeded in 96-well plates at a density of 60,000 cells/$cm^2$ and cultured in DMEM (Gibco™, Walthan, Massachusetts, USA), supplemented with 10% FBS (Corning Cellgro, Manassas, VA, USA), 1% Glutagro™ (Corning Cellgro, Manassas, VA, USA) and 1% Penicillin/Streptomycin solution (Corning Cellgro, Manassas, VA, USA). Primary TSPCs were seeded in 96-well plates at a density of 3,000 cells/$cm^2$ and cultured in α-MEM (Corning, NY, USA) supplemented with 10% FBS (Corning Cellgro, Manassas, VA, USA), 1% Glutagro™ (Corning Cellgro, Manassas, VA, USA) and 1% Penicillin/Streptomycin solution (Corning Cellgro, Manassas, VA, USA). Cells were left to adhere for 24 h in an incubator with a humidified atmosphere, containing 5% $CO_2$ and 95% air, and then treated with decreasing concentrations (0.1 mg/mL, 0.05 mg/mL and 0.001 mg/mL) of PC empty nano-vesicles obtained with both TF-UF and MF. After 24 h and 72 h, cells metabolic activity was analyzed using the 3-(4,5-Dimethylthiazol-2-yl)-2,5-diphenyltetrazolium bromide (MTT) assay. MTT was added (0.5 mg/mL) to each well and incubated at 37 °C for additional 4 h. Supernatants were completely removed, and formazan products were dissolved in 100 μl of dimethyl sulfoxide (DMSO). Absorbance was determined at 570 nm using a microplate reader (Infinite F200 PRO, Tecan Group Ltd., SW). All assays were performed in triplicate, each one on a single subject (N = 3). Cells metabolic activity was calculated as a percentage with respect to the control group (considered as 100%), according to Eq. (3):

$$\text{Cells metabolic activity}\,(\%) = \frac{Abs\ of\ sample - Abs\ of\ blank}{Abs\ of\ control - Abs\ of\ blank} \text{ x } 100 \quad (3)$$

### 2.8. Cellular uptake by immunofluorescence assay in 2D and 3D culture

PC/FITC loaded vesicles were prepared and used to monitor carriers' cellular uptake (both HeLa and TSPCs) using immunofluorescence (IF) imaging in 2D and 3D culture.

Regarding 2D culture, HeLa cell line and primary hTSPCs were seeded in 12-well plates at a density of 4,000 cells/$cm^2$ and cultured, respectively, in DMEM (Gibco™, Walthan, Massachusetts, USA) and α-MEM (Corning, NY, USA), both supplemented with 10% FBS (Corning Cellgro, Manassas, VA, USA), 1% Glutagro™ (Corning Cellgro,

**Table 1**
Mean Sizes, standard deviation, Zeta potential, and drug loading (T3 or FITC) of PC nano-vesicles obtained by *Microfluidic (MF), Thin Film Hydration plus ultrasonication/filtration (TF-UF)* and *Supercritical Liposome Formation Technique (SC)*. Values are reported as means ± standard deviation (SD) (n = 3).

| Supercritical Liposome Formation Technique (SC) | | | | | | | |
|---|---|---|---|---|---|---|---|
| Composition | **O/W ratio** | **P/T** | **Mean Diameter** | **Zeta potential (mV)** | **Loading (mg/$g_P$)** | **EE%** | **Ethanol Residue** |
| | | **MPa/°C** | **(nm)** | | | **(%%)** | **(ppm)** |
| PC | 1:3 | 150/38 °C | 179.9 ± 95 | − 4.18 | – | | 580 |
| PC/T3 | 1:3 | 150/38 °C | 234 ± 143 | − 6.50 | 1 | 10 | 890 |
| PC/FITC | 1:3 | 150/38 °C | 285 ± 111 | − 7.22 | 8 | 90 | 800 |
| Thin Film Hydration plus ultrasonication/filtration (TF-UF) | | | | | | | |
| Composition | **Sonication** | **Filter mesh** | **Mean Diameter** | **Zeta potential (mV)** | **Loading (mg/g)** | **EE%** | **Ethanol Residue** |
| | **sec** | **μm** | **(nm)** | | | **(%%)** | **(ppm)** |
| PC | 120 s | 0.22 | 179.9 ± 95 | − 4.18 ± 1.23 | – | | – |
| PC/T3 | 120 s | 0.22 | 167.7 ± 90 | − 8.50 ± 0.60 | 10 | 58 | – |
| PC/FITC | 120 s | 0.22 | 183.7 ± 96 | − 8.42 ± 0.88 | 5 | 80 | – |
| Microfluidic (MF) | | | | | | | |
| Composition | **m)O/W ratio** | **TFR** | **Mean Diameter (nm)** | **ZetaP (mV)** | **Loading (mg/g)** | **EE%** | **Ethanol Residue** |
| | | **mL/min** | | | | **(%%)** | **(ppm)** |
| PC | 1:3 | 6 | 55.35 ± 31 | −21.5 ± 5.91 | – | | 1400 |
| PC/T3 | 1:3 | 6 | 102.9 ± 48 | −21.0 ± 6.69 | 11 | 58 | 1510 |
| PC/FITC | 1:3 | 6 | 50.02 ± 25 | −21.6 ± 7.32 | 5 | 70 | 1390 |
| PC | 1:3 | 8 | 44.64 ± 23 | −14.0 ± 5.88 | – | | 1490 |
| PC/T3 | 1:3 | 8 | 88.61 ± 44 | −20.1 ± 5.90 | 10 | 57 | 1600 |
| PC/FITC | 1:3 | 8 | 41.03 ± 24 | –23.8 ± 7.04 | 5 | 65 | 1389 |

Manassas, VA, USA) and 1% Penicillin/Streptomycin solution (Corning Cellgro, Manassas, VA, USA). Cells were left to adhere for 24 h in an incubator with a humidified atmosphere, containing 5% $CO_2$ and 95% air, and then treated with MF vesicles at 0.1 mg/mL (HeLa) and 0.001 mg/mL (hTSPCs). After the incubation time (24 h for HeLa and 72 h for hTSPCs), cells were fixed with 3.7% formaldehyde for 30 min at room temperature (RT) followed by permeabilization with 0.1% Triton X-100 for 5 min and blocking with 1% BSA for 1 h. For β-actin staining, cells were incubated for 1 h at RT with a mouse monoclonal anti-β actin antibody (1:100, Cell Signaling Technology, Danvers, Massachusetts, USA). Following incubation with the primary antibody, cells were incubated for 1 h at RT with the Alexa Fluor™ plus 594 goat anti-mouse IgG (1:500; Thermo Fisher Scientific, Waltham, MA, USA) antibody. Cell nuclei were stained with DAPI solution (1:1000) for 5 min. All images were acquired at 20x magnification with identical settings of light, exposure time, and gain using a fluorescence microscope (Eclipse Ti Nikon Corporation, Tokyo, Japan) (Pireddu et al., 2018).

Concerning 3D culture, high-density cultures were obtained using 96 wells ultra-low attachment microplates (Corning, Manassas, VA, United States). Briefly, hTSPCs were resuspended at a density of 500.000 cells/ml. 100 μl of cell suspension were dispensed in each well and, after 5 days, the resulting cellular aggregates were treated with MF vesicles at 0.001 mg/mL for 7 days. After the incubation time, cells were fixed with 3.7% formaldehyde overnight at 4 °C using a tubes rotator (LLG-Labware, Meckenheim, Germany) followed by permeabilization with 0.5% Triton X-100 (30 min at RT on rotator) and blocking with 2% BSA plus 0.1% Triton X-100 (1 h at RT on rotator). For type I Collagen staining, cells were incubated with a mouse monoclonal anti-type I Collagen antibody (1:100; Sigma Aldrich, St. Louis, MO, USA) overnight at 4 °C on rotator. Following incubation with the primary antibody, cells were incubated for 3 h at RT on rotator with the Alexa Fluor™ plus 594 goat anti-mouse IgG (1:500; Thermo Fisher Scientific, Waltham, MA, USA) antibody. Cell nuclei were stained with DAPI solution (1:1000) for 20 min on rotator. All images were acquired at 20x magnification with identical settings of light, exposure time, and gain using Leica laser-scanning confocal microscope (mod. TCS SP5; Leica Microsystems, Wetzlar DE).

3D systems morphology was monitored on brightfield images with the ImageJ software (rel.1.52p National Institutes of Health, USA). The diameter, area (A) and perimeter (p) were measured, and circularity was calculated using the equation (4):

$$\text{F circularity} = \frac{4\pi A}{p^2} \quad (4)$$

For the evaluation of Feret's diameter and circularity, the average value of three 3D-systems (n = 3), were considered (De Moor et al., 2020).

### 2.9. Brightfield images

Brightfield images were captured at different time points at 5x magnification using a Leica DMIL LED microscope and acquired by Leica DFC425 C Camera.

### 2.10. Biological activity by gene expression in 2D and 3D culture

RNA was extracted from both 2D and 3D culture of *h*TPSCs using the RNeasy Mini Kit (Qiagen, DE). 1 μg of total RNA for each sample was *retro*-transcripted with the iScript™ cDNA synthesis kit (Bio-Rad, Milan, IT). Relative gene expression analysis was performed in a LightCycler® 480 Instrument (Roche, IT), using the SsoAdvanced™ Universal SYBR® Green Supermix (Bio-Rad) and the validated primers for SCX-A, COL1A1, COL3A1, DCN and TNC (Bio-Rad), according to MIQE guidelines (Bustin et al., 2009). Triplicate experiments were performed for each condition studied and data normalized to GAPDH expression. The geNorm method (Hellemans et al., 2007) was applied to calculate reference gene stability between the different conditions (calculated with CFX Manager software; M < 0.5). Fold changes were determined using the $2^{-\Delta\Delta Ct}$ method and presented as relative levels over T0 (2D or 3D culture) = 1.

### 2.11. Statistical analysis

Statistical analysis was performed using GraphPad Prism software (v6.0 for Windows, LLC, San Diego, California, United States). Data obtained from multiple experiments (n = 3) were calculated as mean+/-

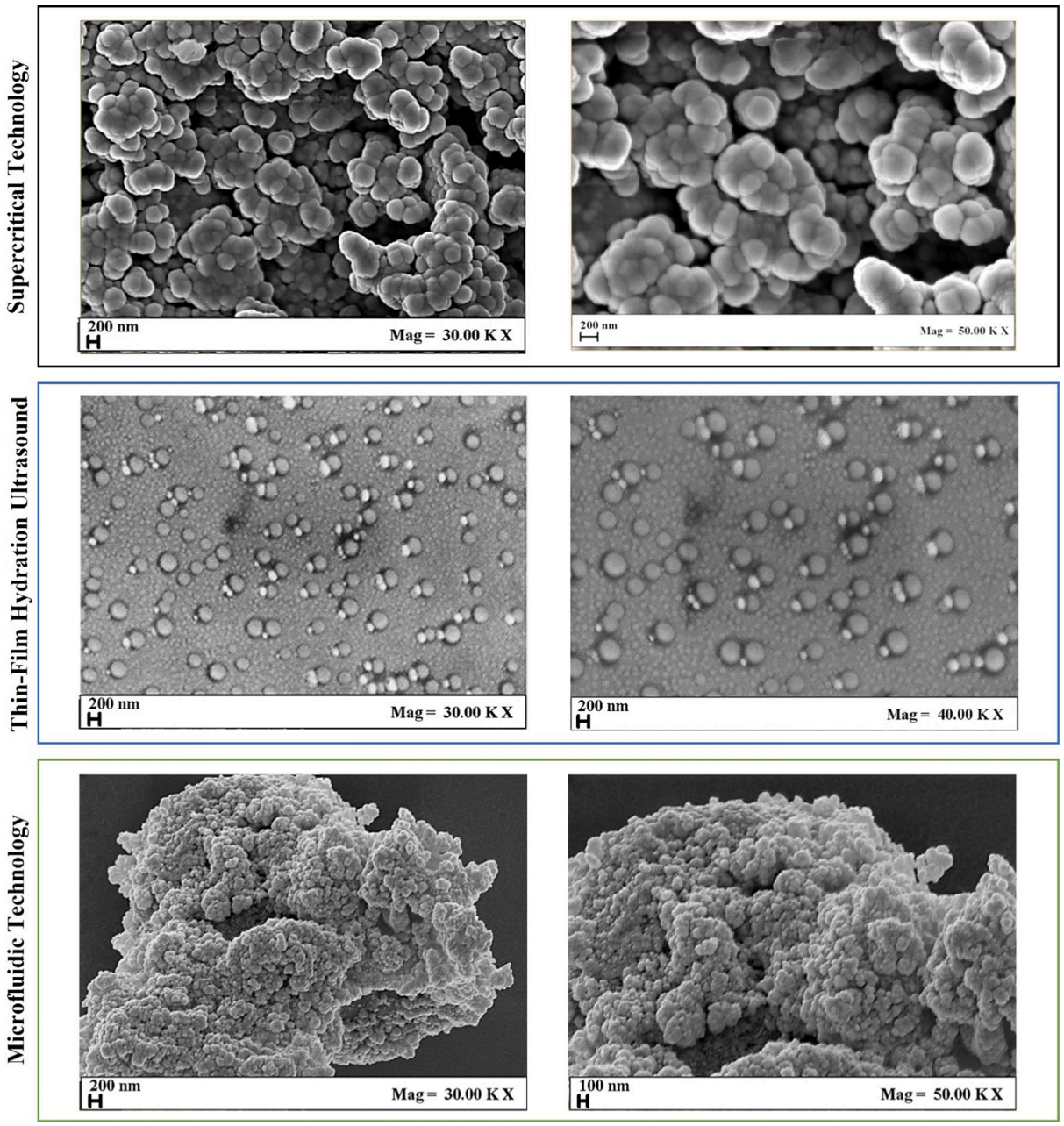


**Fig. 2. Field-Emission Scanning Electron Microscopy micrographs of PC vesicles obtained by different technologies.** SC fabricated vesicles showed the largest size with a well-shaped structure, even if aggregates were observed due to the preparation methods. Well-shaped spherical vesicles were obtained by TF-UF method. The smallest vesicles appeared to be the ones prepared using MF technology even if they partially collapsed during the freeze-drying preparative protocol and huge aggregated were observed.

SD and analyzed for statistical significance using a nonparametric one-way ANOVA test, for independent groups. Differences were considered statistically significant when $p < 0.05$.

## 3. Results and discussion

### 3.1. Nano-vesicle fabrication and characterization

In order to explore different technologies for nano-vesicle fabrication, a relatively simple composition of the lipid phase was adopted selecting only one phospholipid, i.e., phosphatidylcholine (PC), that was also previously investigated for the fabrication of nano-vesicles used for cellular uptake (Ciaglia et al 2019). Furthermore, because the T3 hormone has a well-known activity after its internalization, it seemed also a good drug candidate to encapsulate within vesicles for exploring their biological activity. T3 has a key role in the metabolism of several organs and tissues, regulating cell morphology, differentiation, and proliferation. Moreover, its specific effects on tendon proteins ECM synthesis and organization have been already described (Berardi et al., 2014; Oliva et al., 2019).

So, PC, PC/T3, and PC/FITC loaded vesicles were prepared adopting three different manufacturing methods and the resulting carriers were compared for size, Zeta potential (Zp), ethanol residue (if applicable), and loading, as summarized in Table 1.

TF-UF was preliminary explored because is the most widely described in the literature (see Fig. 1). Resulting vesicles showed a well-defined spherical shape with mean sizes ranging between 167 ± 90 nm (empty) and 183 ± 96 nm (T3 loaded) and Zp values between −4 and

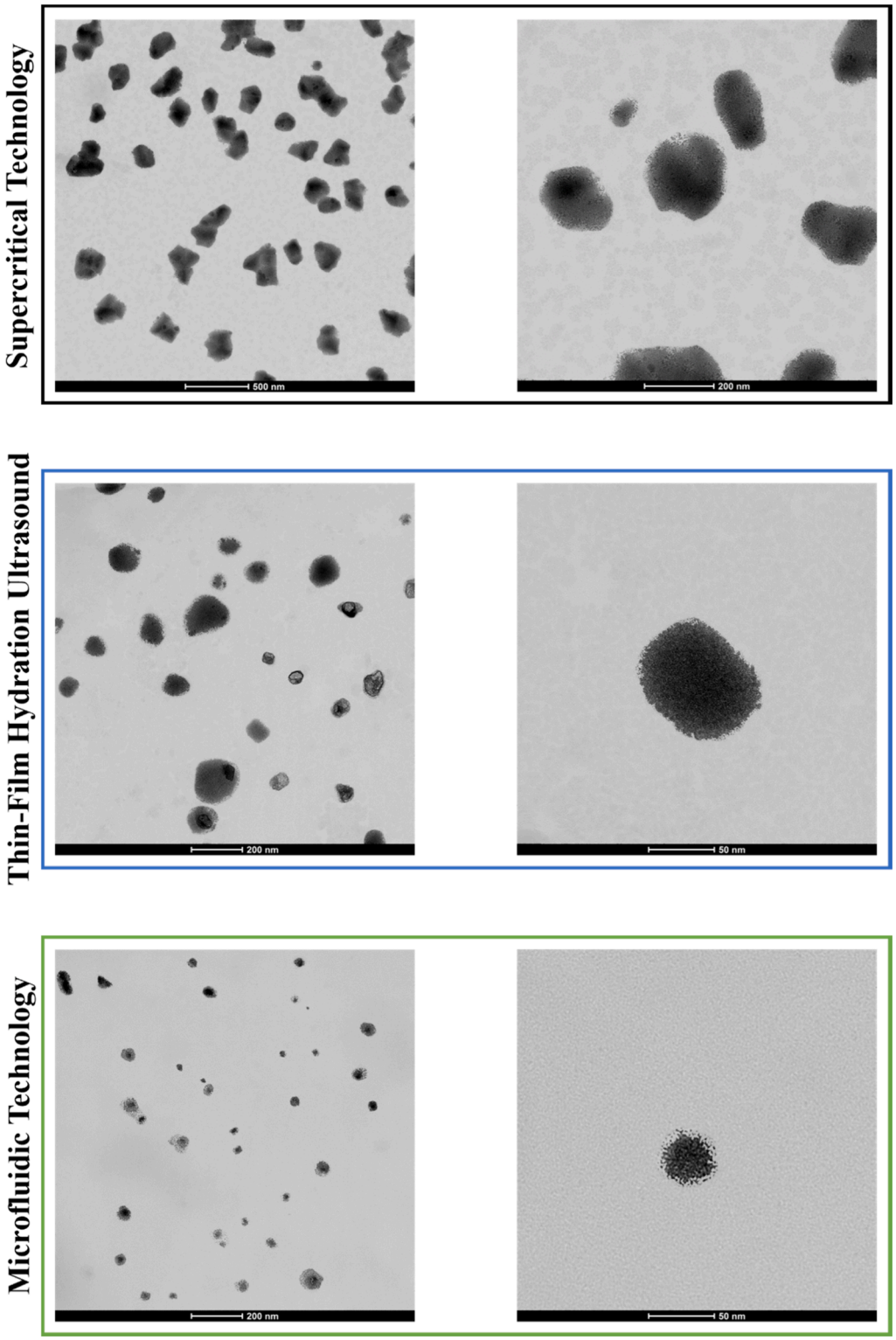


**Fig. 3.** TEM bright-field micrographs of PC vesicles obtained by different technologies. The magnification scale is shown at the bottom of each micrograph.

−8 mV. T3 loading was 10 mg/g due to an encapsulation efficiency of about 60%. Despite the good vesicle sizes and loading, this protocol had several drawbacks such as the film hydration and the ultra-sonication step, which can cause both drug degradation and low overall yield (Meure et al., 2008). Indeed, in our case, a mean value of 50% w/w of mass loss was observed.

SC technology or dense gas-based processes were largely described to fabricate lipid nanoparticles (Campardelli et al., 2013, 2016; Espirito Santo et al., 2014, 2015); these processes were also reported to assure an extremely narrow particle size distribution coupled with a low solvent residue (Campardelli et al., 2012; Della Porta et al., 2013) and a continuous workflow processing (Della Porta et al., 2011). Pressure and temperature operative condition were already optimized (Ciaglia et al 2019) and largely documented in the literature. In such case, PC/T3 and PC-empty vesicles with a mean size of 285 ± 111 and 179 ± 90 nm, were obtained, respectively; Zp values ranged between −4 and −7 mV.

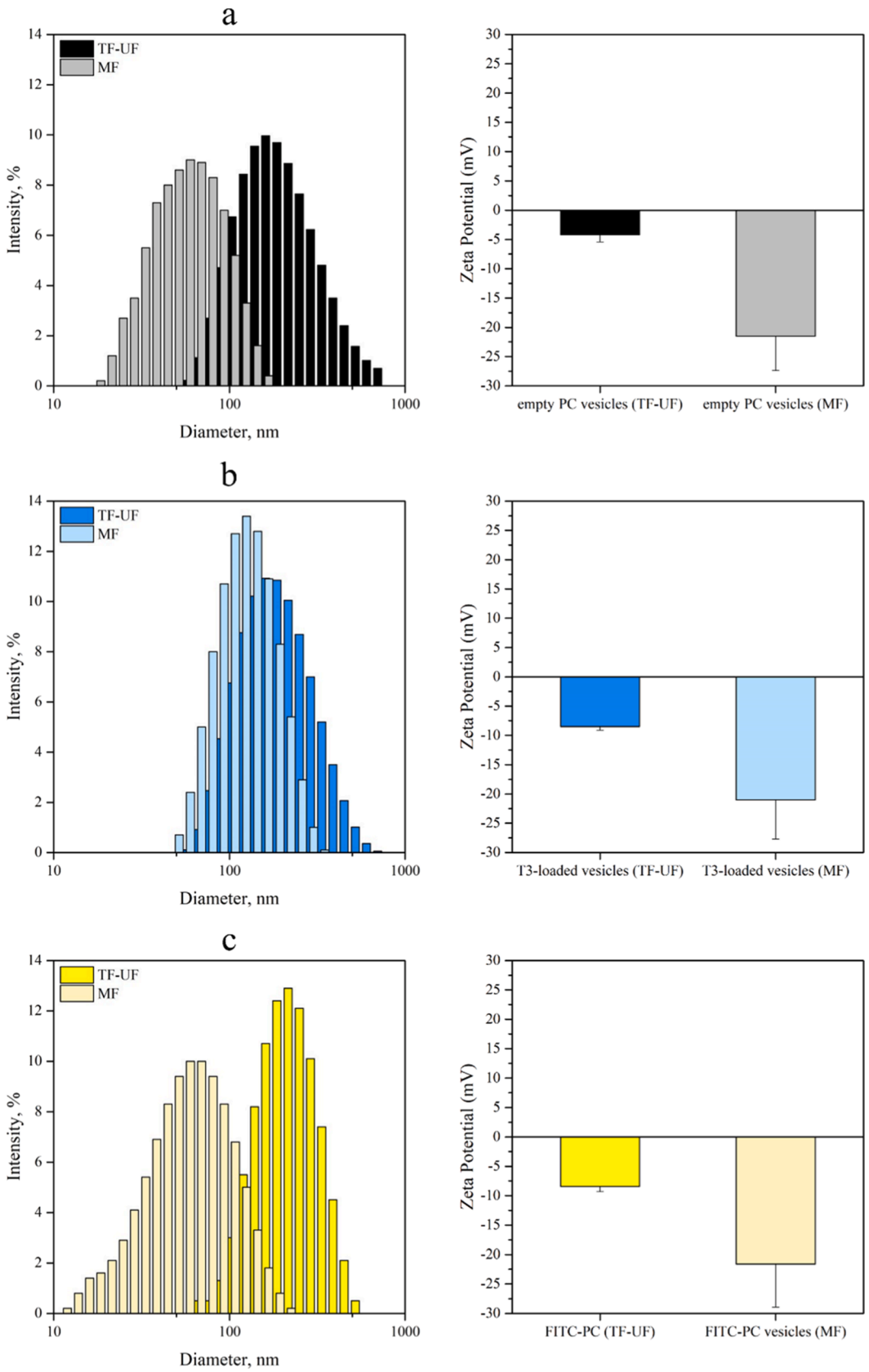


**Fig. 4. Size distributions and zeta potential of PC vesicles obtained by different technologies.** Comparison between empty PC vesicles **(a),** T3-loaded PC vesicles **(b)** and FITC-loaded PC vesicles, obtained with Thin Film Hydration coupled to ultrasonication/filtration (TF-UF) and Microfluidic (MF) fabrication methods. The smallest mean size with the narrowest distribution was obtained using MF technology at the conditions explored. SC fabricated vesicles were not further considered because of the extremely poor loading of T3, probably due to a drug extraction by the ethanol/supercritical carbon dioxide mixture.

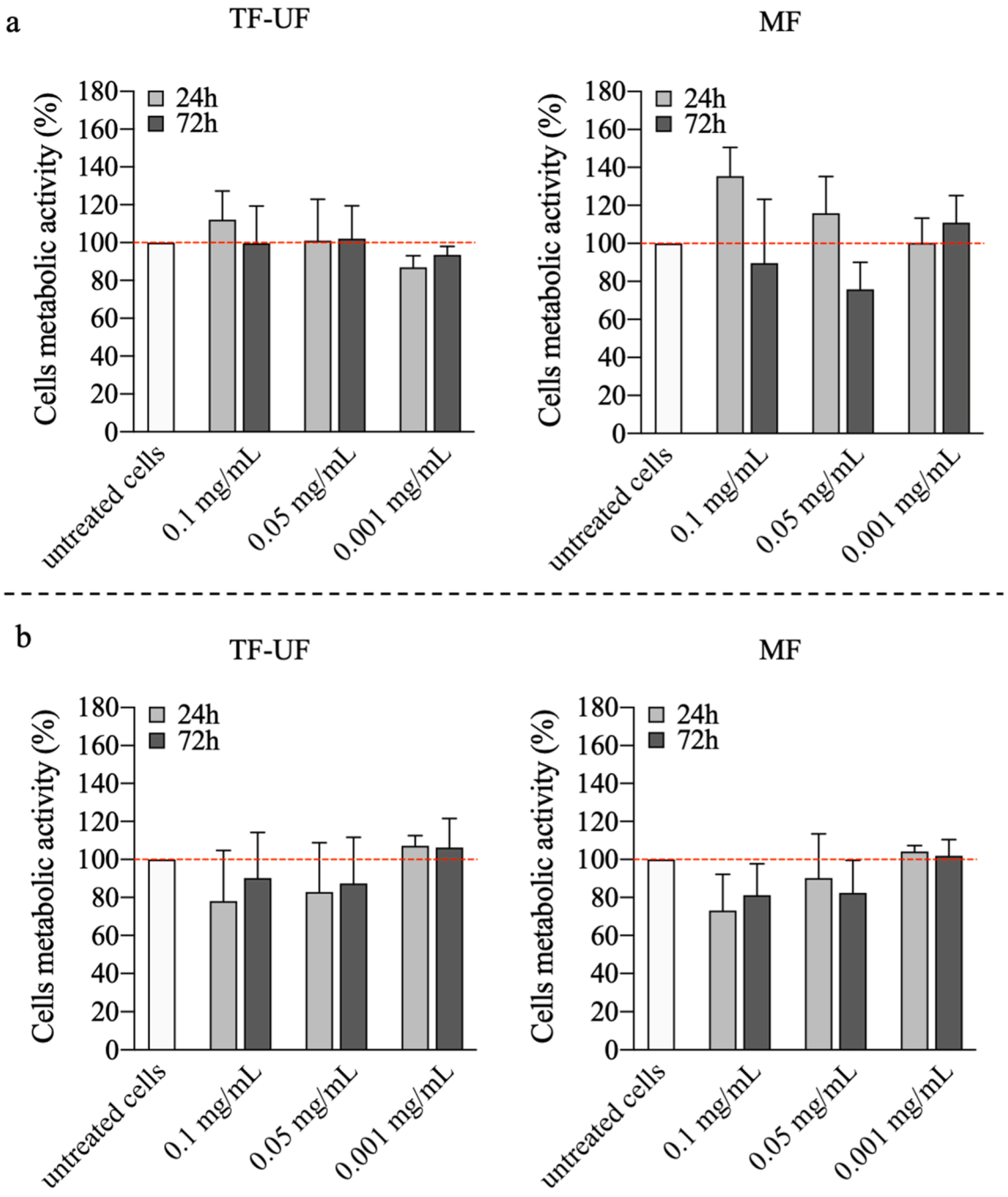


**Fig. 5. Cytotoxicity study.** Cells metabolic activity was measured by MTT assay on HeLa (**a**) and TSPCs (**b**) treated with decreasing concentration of PC empty nano-vesicles obtained with both Thin Film Hydration coupled to ultrasonication/filtration (TF-UF) and Microfluidic (MF) (N = 3).

Despite the good vesicle shape and distribution, in the case of T3 encapsulation, the efficiency was extremely poor (<10%). This low performance can sometimes occur and it was also already described when the biomolecule, which has to be loaded into a specific nanocarrier (in our case T3), is particularly soluble in dense carbon dioxide or in the dense mixture of solvent/ carbon dioxide that is formed along the process evolution. In these unlucky conditions the encapsulation efficiency is often poor or extremely low due to a huge drug loss in the downstream current continuously flowing out of the reactor (see Fig. 1). This drawback, in our case, can be probably due because T3 is slightly hydrophobic molecules that was added to a mixture of ethanol and carbon dioxide obtaining a complex vapor–liquid mixture behavior, that may promote the drug extraction from the overall mixtures such as water/ ethanol/CO2 rather than its precipitation/collection in the polymer or vesicles within the water phase (Falco et al., 2013; Gimenez-Rota et al., 2019). In these adverse cases, the vapor–liquid equilibrium (VLE) of the complex mixture (formed by the organic solvent, water, dense carbon dioxide, and solutes) at given pressure and temperature conditions are often unknown, and, therefore, the system is quite difficult to be managed. It is also possible to find out a specific pressure/temperature condition in which the solutes are not extracted, however, due to the thermal potential degradation of the drug, not all the temperatures can be explored and used. Often, an empirical approach is adopted and it can include the performing of several runs at different solute compositions and pressure/temperature conditions but in our particular case, the temperature values that can be explored must be lower than 38 °C to avoid nano-vesicles aggregations. Taking into account these particularly adverse conditions the SC technology was not further explored.

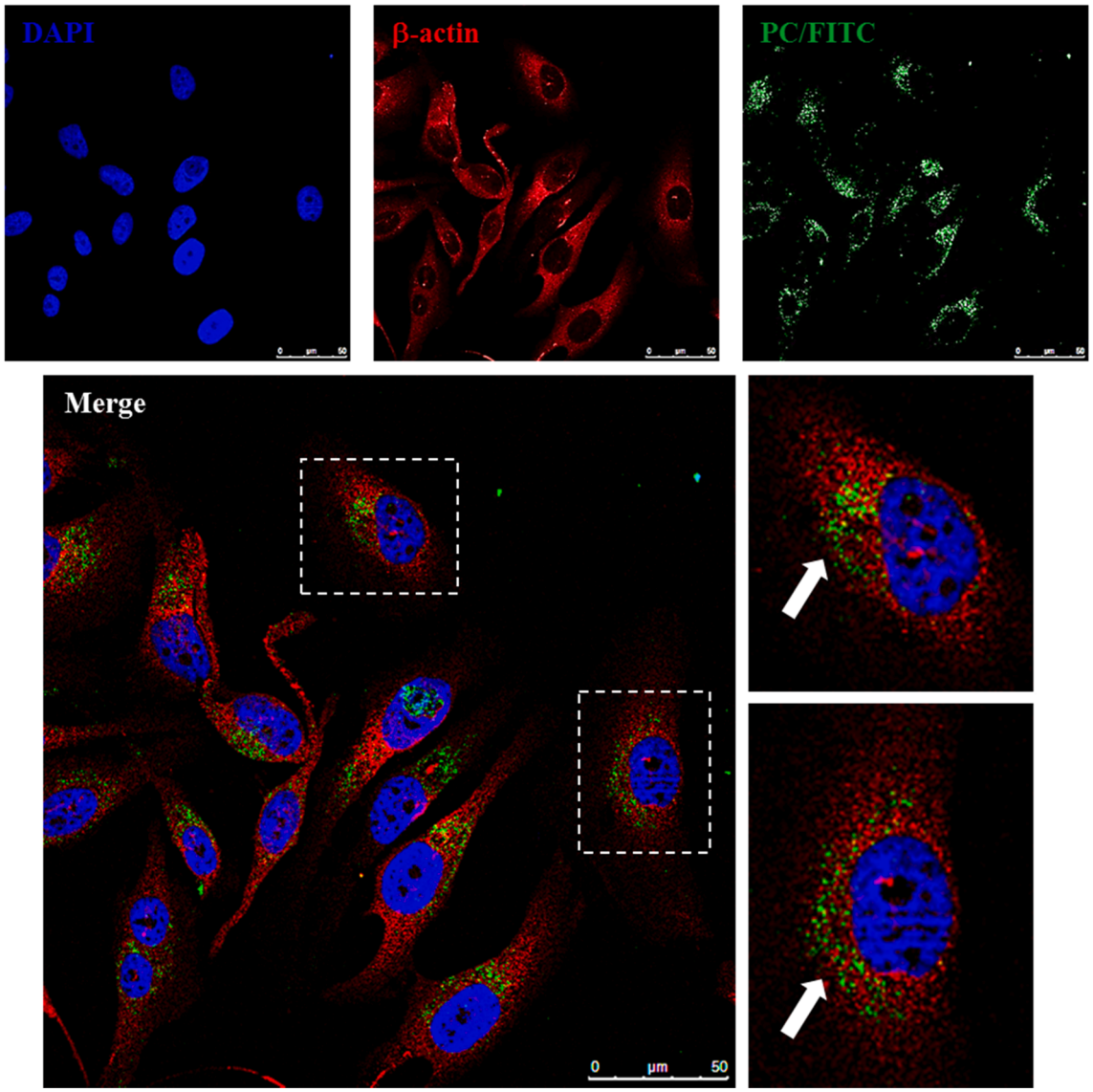


**Fig. 6. Vesicles internalization in HeLa cell line.** Confocal microscope images of HeLa cell line incubated with a media having MF vesicles at concentration of **0.1 mg/mL**, that was measured to be the highest vesicles concentration that not properly affected cells viability. HeLa cytoplasm was highlighted monitoring the β-actin (red) and the vesicles internalization events (green) were observed just after 24 h. DAPI was used to counterstain cells nuclei (blue). Scale bar = 50 µm.

MF protocol requires ethanol and water solutions mixed by means of the microfluidic circuit. T3 and PC were dissolved into ethanol and then mixed into the water phase (ratio 1:3); a total flow rate of 6 or 8 mL/min was explored. The Y-shaped microcircuit selected had a length of 20 mm and an internal diameter of 0.6 mm (see Fig. 1). Dialysis step for ethanol and not-encapsulated T3 elimination was adopted, without further post-processing steps (Dikpati et al., 2020). Vesicles with a mean size ranging from 55.35 ± 31 (empty) and 102.9 ± 48 nm (T3 loaded) and Zp values between −20 and −21 mV were obtained. A T3 loading of 10 mg/g was obtained with a good encapsulation efficiency of almost 60%.

FE-SEM images of all nano-vesicles obtained are also reported in Fig. 2**.** Well-shaped spherical systems were observed for all the technologies explored, even if a smooth surface was observed for the ones obtained by TF-UF, whereas, irregular surfaces were identified for SC-vesicles. This is probably due to a pressure gap they had during the recovery step from the high-pressure reactor to the separator, working at atmospheric pressure (Espirito Santo et al., 2014, 2015). MF fabricated nano-vesicles were the smallest and, therefore, large aggregates were observed, probably formed during the drying step on the microscope stub. To better characterize the size and morphology of different liposomes, TEM analysis was also performed as it can directly display single liposomes of the suspension and even their architecture, without promoting aggregation processes during samples preparation. Findings are shown in Fig. 3 and are congruent to DLS data, confirming that after the microfluidic process the smallest and most homogeneous liposomes were obtained, with a SUV structure.

Ethanol residue was also monitored when present (see Table 1); the higher solvent retention was observed in the vesicles suspension fabricated by MF technology and the maximum value measured was 1500 ppm, after the dialysis step; SC technology is well-known to provide extremely low solvent residue (Espirito Santo et al., 2014, 2015) and also in this case values between 800 and 600 ppm were measured. Despite this nice outcome, due to extremely poor drug loading, this technology was not further considered in the present work.

Vesicle size distributions and zeta potential obtained by TF-UF and MF were compared in Fig. 4**.** Images show that MF technology allowed the fabrication of the narrowest distribution, the smallest vesicles. When T3 was successfully loaded in vesicles fabricated (with both technologies), the vesicles mean size increased, probably due to the physical volume required for T3 hosting within the structure.

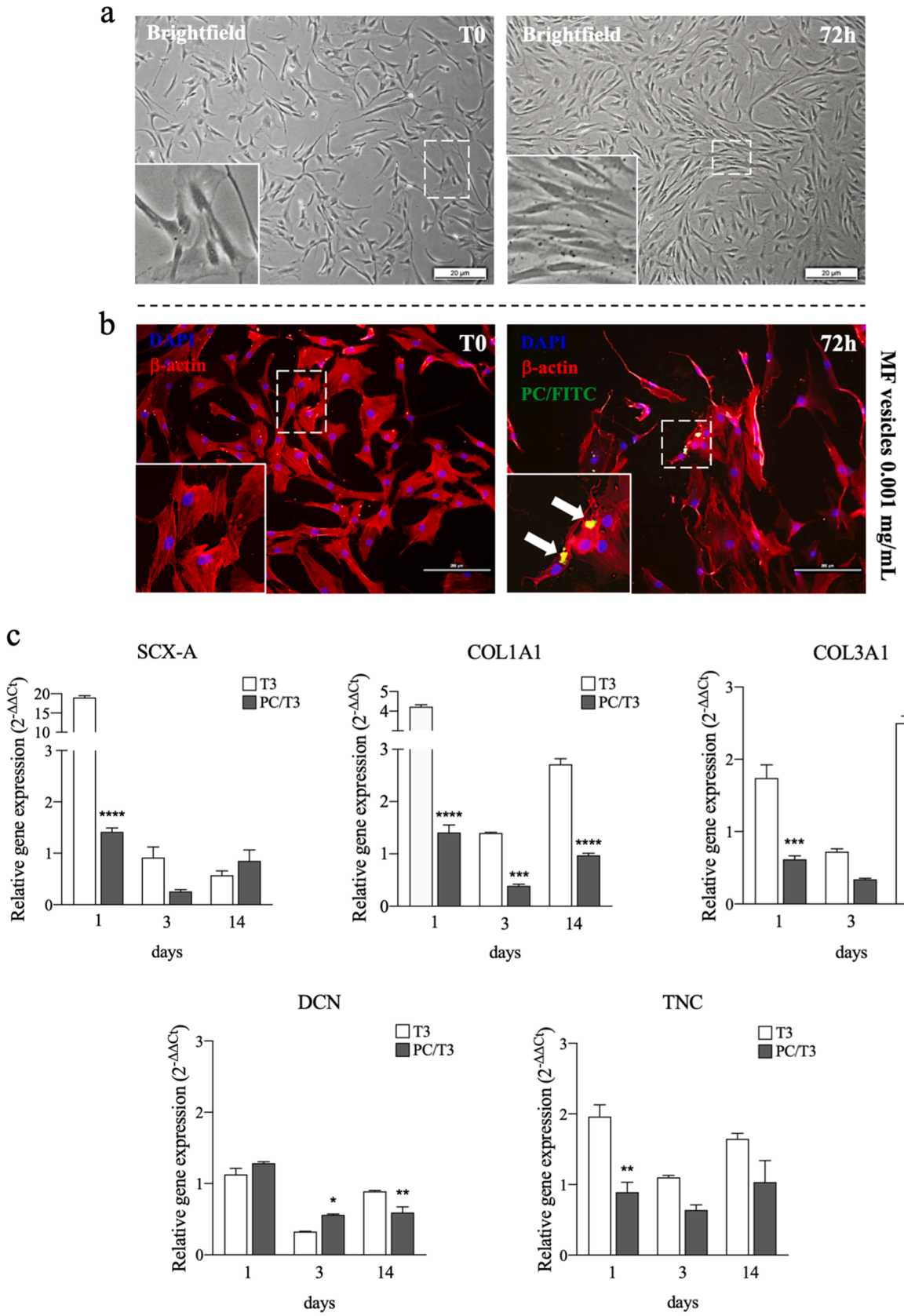


**Fig. 7. Vesicles internalization in 2D TSPCs culture and gene expression profile.** Brightfield (**a**) and immunofluorescence (**b**) microscope images of TPSCs primary cell line incubated with MF vesicles at concentration of **0.001 mg/mL.** The cytoplasm was highlighted monitoring the β-actin (red) and internalization events (green) were observed again after 72 h. Gene expression profiles (**c**) for tenogenic markers (Scleraxis, SCX-A; type III Collagen, COL3A1; Decorin, DCN; Tenascin, TNC) of Tendon Stem/Progenitor cells (TSPCs) cultured up to 14 days in a medium supplemented with vesicles fabricated by Microfluidic (MF) is also reported. * $p < 0.05$, ** $p < 0.01$, *** $p < 0.001$ and **** $p < 0.0001$ ($N = 3$). Scale bar: 20 μm for brightfield and 200 μm for immunofluorescence images.

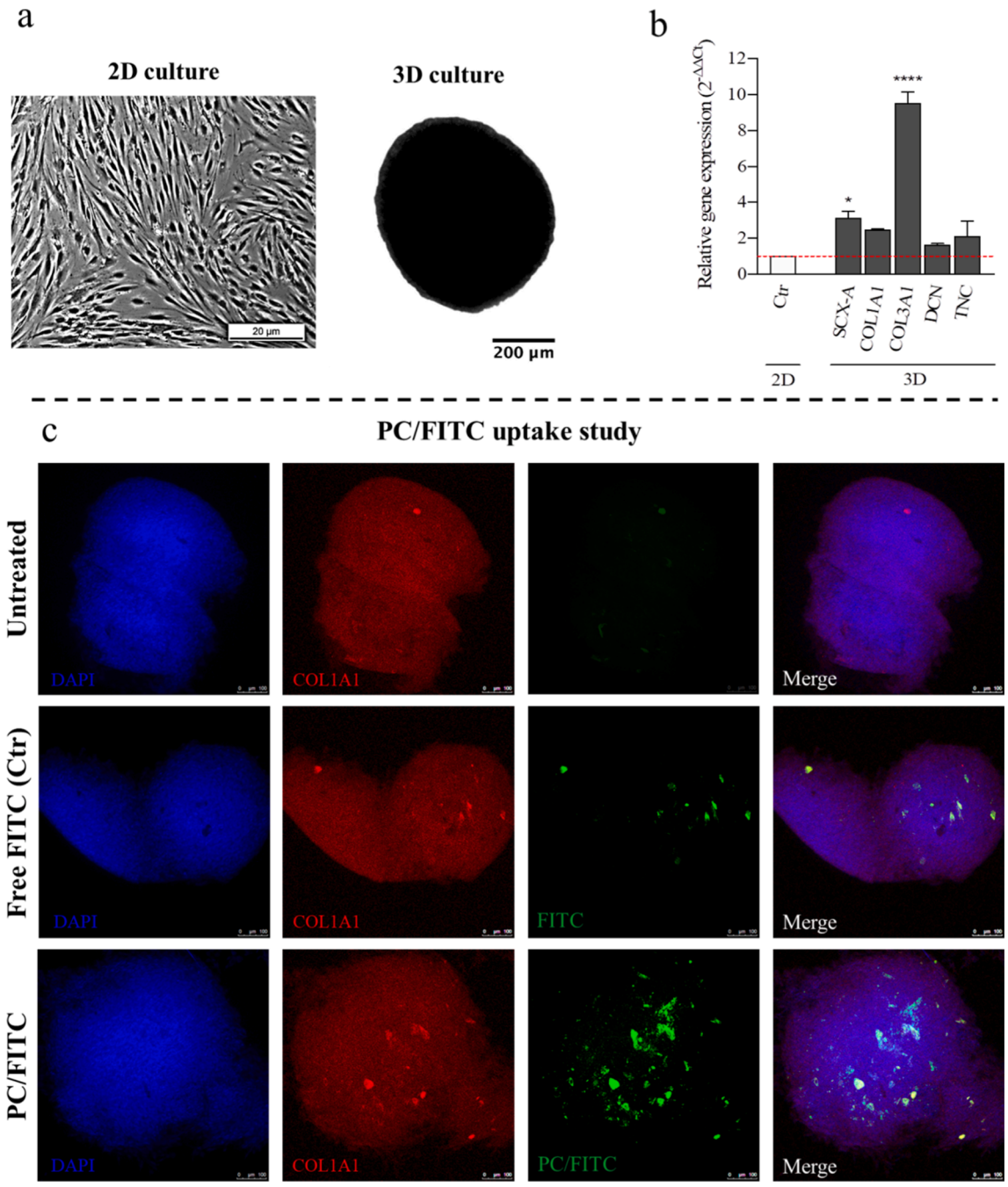


**Fig. 8. TSPCs culture, gene expression profile, and PC/FITC vesicles internalization.** Brightfield images of 2D and 3D TPSCs culture, just after high-density culture formation (**a**). Gene expression profiles for tenogenic markers (Scleraxis, SCX-A; type I and type III Collagen, COL1A1 and COL3A1; Decorin, DCN; Tenascin, TNC) of Tendon Stem/Progenitor cells (TSPCs) cultured in 3D (**b**). Immunofluorescence images of 3D TPSCs culture after incubation for 7 days with PC/FITC vesicles at concentration of **0.001 mg/mL;** soluble and free FITC was used as control. The cytoplasm was highlighted monitoring type I Collagen (red) and internalization events (green) were observed after 7 days (**c**). * $p < 0.05$, ** $p < 0.01$, *** $p < 0.001$ and **** $p < 0.0001$ ($n = 3$). Scale bar: 20 µm for brightfield and 100 µm for immunofluorescence images.

Despite similar loading and good sizes in both technologies explored, the microfluidic one seemed to provide a faster and easier fabrication protocol coupled with better control of vesicles size distribution and excellent batch-to-batch reproducibility. Furthermore, for the specific application studied, smaller vesicles with narrower size distribution seemed to be more suitable because those parameters strongly affect the cellular uptake mechanism (Andar et al., 2014; Sercombe et al., 2015). Z-potential analysis showed that MF vesicles had also the greatest positive surface charge (Zp of $-20.1 \pm 5.90$), suggesting that these vesicles had an excellent repulsion force that will prevent their aggregation process and improve their shelf-life. Additionally, this Zp value was indicated as the best for the mechanism of cellular internalization (Honary and Zahir, 2013). Finally, the ethanol residue was successfully reduced by dialysis step to about 1300–1400 ppm; these values seemed suitable for further investigations reported below.

### 3.2. Cytotoxicity studies

In vitro toxicity of TF-UF and MF vesicles formulations was performed to identify eventual harmful concentrations before the

internalization study. Two different cell types, the HeLa cell line and human primary Tendon Progenitor Stem Cells (hTPSCs), isolated by human explants, were used and underwent the MTT assay. Taking into account that cytotoxicity effects strongly depend on different parameters, such as phospholipids and their concentration as well as manufacturing process (Kirchner et al., 2005), a decreasing concentration of PC (0.1 mg/mL, 0.05 mg/mL, 0.001 mg/mL) of both TF-UF and MF nano-vesicles was used, and cells metabolic activity was monitored after 24 h and 72 h (see Fig. 5a-b). Supplementing vesicle concentrations equal to or lower than 0.1 mg/mL, both cell types maintained their metabolic activity, reaching 80–100% after 24 h and 72 hr in the case of TPSCs treated with both TF-UF and MF vesicles. Data indicated that at these concentrations cell viability was excellent. However, it was even better in hTPSCs when both TF-UF and MF vesicles were supplemented at a concentration of 0.01 mg/mL (Fig. 5b).

This information is particularly important because we have to consider that the therapeutic concentration of supplemented vesicles, able to ensure the biological effect of T3 on the cells, could be near the lowest one tested, as previously optimized (Berardi et al., 2014).

Following all these data, and despite liposome formulations may be prepared by adopting other technologies, the MF method was particularly suitable in our specific case because it seemed faster and more reproducible than the TF-UF, which instead required several post-processing steps. Consequently, MF fabricated vesicles were selected for cellular uptake studies.

### 3.3. Cellular uptake observations and biological activity

Cellular internalization studies were performed using PC/FITC vesicles fabricated by MF technology and adopting different concentrations. Preliminary data using PC/FITC vesicles were acquired on a HeLa cell line incubated with a media having a vesicle concentration of 0.1 mg/mL. Internalization events after 24 h were observed by confocal microscope as reported in Fig. 6. Vesicles were grouped within the cytoplasm and in the surrounding cell nuclei; furthermore, cells always appeared healthy, maintaining their typical morphology.

In the case of TPSCs primary cells, that showed a fibroblast-like elongated shape (Fig. 7a), 0.001 mg/mL of PC/FITC vesicles was adopted to monitor the internalization, referring to this concentration as the one expected for the T3 loaded in vesicles able to show a biological effect, as previously described and optimized by Berardi and co-workers (Berardi et al., 2014). In this last case, even if extremely diluted, the vesicles were again successfully observed in cell cytoplasm after 24 h of supplementation. However, their fluorescent signal was less evident because of the lower concentration used, as indicated in Fig. 7b (see arrowheads).

Finally, TSPCs cultures were supplemented with PC/T3 nano-vesicles; free T3 hormone was used for control purposes at a concentration of $10^{-6}$ M, described as the best to promote tenogenic genes overexpression, such as *type III Collagen*, *Decorin*, and *Tenascin-C* (Berardi et al., 2014; Ciardulli et al., 2022). The transcription factor *Scleraxis-A* was also assayed. The overall gene expression was monitored by q-RT-PCR and reported in Fig. 7c, in the case of 2D culture. In such a case, better overexpression was observed in the control group treated with free soluble T3, for almost all the genes monitored, except in the case of *DCN* (0.6-fold; $p < 0.05$) at day 3. Upregulation of the transcription factor *SCX-A* (1.5-fold; $p < 0.0001$) after 24 h was also evident and statistically significant, even if lower than hTSPCs treated with free T3. The statistically significant downregulation of *type III Collagen* appeared as a good result because this type of collagen is often overexpressed by impaired metabolism in pathological cells (Ciardulli et al., 2022). 3D culture was assembled (Fig. 8a) and used to to better check T3/PC vesicle biological behavior; indeed, in such type of 3D cells organization, hTSPCs overexpressed better their constitutive genes (see Fig. 8b); therefore, it seemed a more proper *in vitro* model for PC/T3 vesicles activity investigation. Furthermore, when FITC-loaded PC

a

| | Feret's diameter (μm) | Circularity |
|---|---|---|
| **untreated** | 599.05 ± 68.84 | 0.87 ± 0.01 |
| **T3** | 687.15 ± 10.12 | 0.86 ± 0.01 |
| **PC/T3** | 669.943 ± 12.65 | 0.85 ± 0.02 |

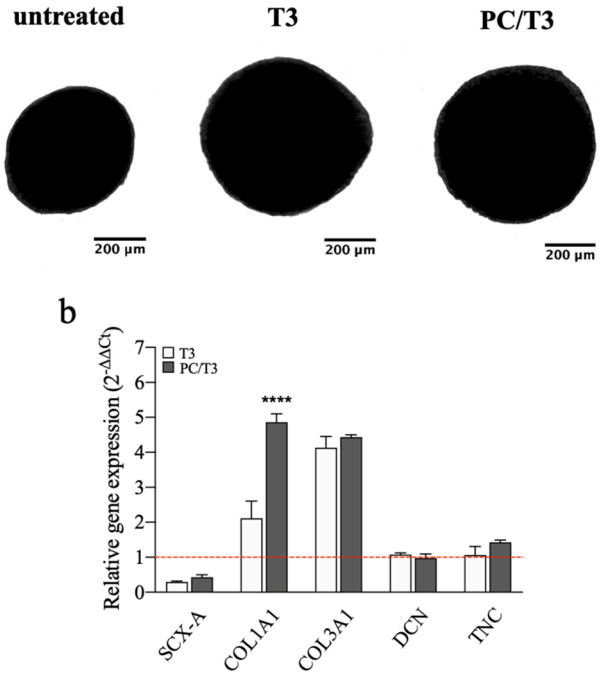


**Fig. 9. Characterization of 3D TPSCs culture treated with MF vesicles and gene expression profile.** Brightfield images of 3D TPSCs culture treated with free-T3 and MF vesicles at concentration of **0.001 mg/mL** for 7 days; relative Feret's diameter and circularity are reported in the Table (**a**). Gene expression profiles for tenogenic markers (Scleraxis, SCX-A; type III Collagen, COL3A1; Decorin, DCN; Tenascin, TNC) of Tendon Stem/Progenitor cells (TSPCs) cultured in 3D (**b**). * $p < 0.05$, ** $p < 0.01$, *** $p < 0.001$ and **** $p < 0.0001$ ($n = 3$). Scale bar: 200 μm.

nanosomes were supplemented to the 3D culture at the same concentration of 0.001 mg/mL, the vesicles retained by the 3D system seemed more abundant, as can be observed in Fig. 8c, where large green areas are evident into the 3D system, compared to control system supplemented with free soluble FITC fluorochrome. When 3D TPSCs culture was supplemented with PC/T3 vesicles, a better spheroids circularity and larger diameter were observed (see Fig. 9a and associated **Table**), coupled to a significant gene over-expression, especially for *COLIA1* (4.8-fold; $p < 0.0001$) at day 7 (Fig. 9b), suggesting a healthier cell culture. The data suggested that T3 maintained its biological activity when entrapped into liposomal formulation; furthermore, PC/T3 formulation increased T3 cytosolic concentration and improved hTPSCs metabolic activity.

## 4. Conclusions

The manuscript reports the fabrication of phosphatidylcholine nanovesicles successfully loaded with T3 hormone using different technologies, such as thin-layer hydration coupled to sonication (TF-UF), supercritical assisted liposome formation (SC), and microfluidic technology (MF). Among them, the microfluidic technology seemed faster, more reproducible, and easier than the conventional thin layer hydration. Vesicles obtained with microfluidic technology were the best

taking into account their small size and narrow distribution, optimal Zp, and drug loading, with also good ethanol residue. SC technology did not provide successful drug loading under explored conditions. Vesicle cytotoxicity and cellular uptake studies suggested an extremely good carrier behavior that also maintained the T3 biological activity on Tendon Stem Progenitor Cells (TPSCs) extracted from human surgery explants. TPSCs 3D culture overexpressed almost all constituent tendon genes also with loaded vesicles supplementation. The study opens perspective for the use of these nano-carriers on *in vivo* models to further explore their versatility in preserving and/or carrying a drug into specific cells or tissues.

## Funding

This research was funded by American Orthopedic Foot & Ankle Society (AOFAS) Research Committee, Grant ID#: 2019-133-S, Grant Project Title: Nano-FT3C+: An Innovative Liposome-Based Formulation for Thyroid Hormone Controlled Delivery. An In Vitro Study on Tendinopathic Human Achilles Tendon Tenocytes".

## CRediT authorship contribution statement

**E.P. Lamparelli:** Data Curation, Investigation, Methodology, Writing – original draft. **M.C. Ciardulli:** Investigation, Methodology. **P. Scala:** Investigation. **M. Scognamiglio:** Formal analysis. **B. Charlier:** Formal analysis. **P. Di Pietro:** Formal analysis. **V. Izzo:** Visualization. **C. Vecchione:** Resources, Visualization. **N. Maffulli:** Methodology, Visualization, Resources. **G. Della Porta:** Conceptualization, Data curation, Funding acquisition, Project Administration, Methodology, Validation, Writing – review & editing. All authors have read and agreed to the published version of the manuscript.

## Declaration of Competing Interest

The authors declare that they have no known competing financial interests or personal relationships that could have appeared to influence the work reported in this paper.

## References

Andar, A.U., Hood, R.R., Vreeland, W.N., DeVoe, D.L., Swaan, P.W., 2014. Microfluidic Preparation of Liposomes to Determine Particle Size Influence on Cellular Uptake Mechanisms. Pharm. Res. 31 (2), 401–413. https://doi.org/10.1007/s11095-013-1171-8.

Arshinova, O.Y., Sanarova, E.V., Lantsova, A.V., Oborotova, N.A., 2012. Lyophilization of liposomal drug forms (Review). Pharm. Chem. J. 46 (4), 228–233. https://doi.org/10.1007/s11094-012-0768-2.

Balazs, D.A., Godbey, W.t., 2011. Liposomes for Use in Gene Delivery. Journal of Drug Delivery 2011, 1–12. https://doi.org/10.1155/2011/326497.

Bangham, A.D., Standish, M.M., Watkins, J.C., 1965. Diffusion of univalent ions across the lamellae of swollen phospholipids. J. Mol. Biol. 13 (1), 238–IN27. https://doi.org/10.1016/S0022-2836(65)80093-6.

Berardi, A.C., Oliva, F., Berardocco, M., la Rovere, M., Accorsi, P., Maffulli, N., 2014. Thyroid hormones increase collagen I and cartilage oligomeric matrix protein (COMP) expression in vitro human tenocytes. Muscles Ligaments Tendons J 4, 285–291.

Bi, Y., Ehirchiou, D., Kilts, T.M., Inkson, C.A., Embree, M.C., Sonoyama, W., Li, L.i., Leet, A.I., Seo, B.-M., Zhang, L.i., Shi, S., Young, M.F., 2007. Identification of tendon stem/progenitor cells and the role of the extracellular matrix in their niche. Nat. Med. 13 (10), 1219–1227. https://doi.org/10.1038/nm1630.

Bozzuto, G., Molinari, A., 2015. Liposomes as nanomedical devices. IJN 975. https://doi.org/10.2147/IJN.S68861.

Bustin, S.A., Benes, V., Garson, J.A., Hellemans, J., Huggett, J., Kubista, M., Mueller, R., Nolan, T., Pfaffl, M.W., Shipley, G.L., Vandesompele, J., Wittwer, C.T., 2009. The MIQE Guidelines: Minimum Information for Publication of Quantitative Real-Time PCR Experiments. Clin. Chem. 55, 611–622. https://doi.org/10.1373/clinchem.2008.112797.

Campardelli, R., Cherain, M., Perfetti, C., Iorio, C., Scognamiglio, M., Reverchon, E., Della Porta, G., 2013. Lipid nanoparticles production by supercritical fluid assisted emulsion–diffusion. The Journal of Supercritical Fluids 82, 34–40. https://doi.org/10.1016/j.supflu.2013.05.020.

Campardelli, R., Della Porta, G., Reverchon, E., 2012. Solvent elimination from polymer nanoparticle suspensions by continuous supercritical extraction. The Journal of Supercritical Fluids 70, 100–105. https://doi.org/10.1016/j.supflu.2012.06.005.

Campardelli, R., Espirito Santo, I., Albuquerque, E.C., de Melo, S.V., Della Porta, G., Reverchon, E., 2016. Efficient encapsulation of proteins in submicro liposomes using a supercritical fluid assisted continuous process. The Journal of Supercritical Fluids 107, 163–169. https://doi.org/10.1016/j.supflu.2015.09.007.

Chacko, I.A., Ghate, V.M., Dsouza, L., Lewis, S.A., 2020. Lipid vesicles: A versatile drug delivery platform for dermal and transdermal applications. Colloids Surf., B 195, 111262. https://doi.org/10.1016/j.colsurfb.2020.111262.

Ciaglia, E., Montella, F., Trucillo, P., Ciardulli, M.C., Di Pietro, P., Amodio, G., Remondelli, P., Vecchione, C., Reverchon, E., Maffulli, N., Puca, A.A., Della Porta, G., 2019. A bioavailability study on microbeads and nanoliposomes fabricated by dense carbon dioxide technologies using human-primary monocytes and flow cytometry assay. Int. J. Pharm. 570, 118686. https://doi.org/10.1016/j.ijpharm.2019.118686.

Ciardulli, M.C., Scala, P., Giudice, V., Santoro, A., Selleri, C., Oliva, F., Maffulli, N., Della Porta, G., 2021. Stem Cells from Healthy and Tendinopathic Human Tendons: morphology, collagen and cytokines expression and their response to T3 thyroid hormone. Cells (MDPI), 2022 accepted.

Cipollaro, L., Trucillo, P., Bragazzi, N.L., Della Porta, G., Reverchon, E., Maffulli, N., 2020. Liposomes for Intra-Articular Analgesic Drug Delivery in Orthopedics: State-of-Art and Future Perspectives. Insights from a Systematic Mini-Review of the Literature. Medicina 56, 423. https://doi.org/10.3390/medicina56090423.

Cosco, D., Paolino, D., Cilurzo, F., Casale, F., Fresta, M., 2012. Gemcitabine and tamoxifen-loaded liposomes as multidrug carriers for the treatment of breast cancer diseases. Int. J. Pharm. 422 (1-2), 229–237. https://doi.org/10.1016/j.ijpharm.2011.10.056.

Danaei, M., Dehghankhold, M., Ataei, S., Hasanzadeh Davarani, F., Javanmard, R., Dokhani, A., Khorasani, S., Mozafari, M.R., 2018. Impact of Particle Size and Polydispersity Index on the Clinical Applications of Lipidic Nanocarrier Systems. Pharmaceutics 10, E57. https://doi.org/10.3390/pharmaceutics10020057.

De Moor, L., Fernandez, S., Vercruysse, C., Tytgat, L., Asadian, M., De Geyter, N., Van Vlierberghe, S., Dubruel, P., Declercq, H., 2020. Hybrid Bioprinting of Chondrogenically Induced Human Mesenchymal Stem Cell Spheroids. Front. Bioeng. Biotechnol. 8, 484. https://doi.org/10.3389/fbioe.2020.00484.

Della Porta, G., Campardelli, R., Falco, N., Reverchon, E., 2011. PLGA microdevices for retinoids sustained release produced by supercritical emulsion extraction: Continuous versus batch operation layouts. J. Pharm. Sci. 100 (10), 4357–4367. https://doi.org/10.1002/jps.22647.

Della Porta, G., Campardelli, R., Reverchon, E., 2013. Monodisperse biopolymer nanoparticles by Continuous Supercritical Emulsion Extraction. The Journal of Supercritical Fluids 76, 67–73. https://doi.org/10.1016/j.supflu.2013.01.009.

di Giacomo, V., Berardocco, M., Gallorini, M., Oliva, F., Colosimo, A., Cataldi, A., Maffulli, N., Berardi, A.C., 2017. Combined supplementation of ascorbic acid and thyroid hormone T3 affects tenocyte proliferation. The effect of ascorbic acid in the production of nitric oxide. Muscles Ligaments Tendons J 7, 11–18. https://doi.org/10.11138/mltj/2017.7.1.011.

Dikpati, A., Mohammadi, F., Greffard, K., Quéant, C., Arnaud, P., Bastiat, G., Rudkowska, I., Bertrand, N., 2020. Residual Solvents in Nanomedicine and Lipid-Based Drug Delivery Systems: a Case Study to Better Understand Processes. Pharm. Res. 37, 149. https://doi.org/10.1007/s11095-020-02877-x.

Espirito Santo, I., Campardelli, R., Albuquerque, E.C., de Melo, S.V., Della Porta, G., Reverchon, E., 2014. Liposomes preparation using a supercritical fluid assisted continuous process. Chem. Eng. J. 249, 153–159. https://doi.org/10.1016/j.cej.2014.03.099.

Espirito Santo, I., Campardelli, R., Albuquerque, E.C., Vieira De Melo, S.A.B., Reverchon, E., Porta, G.D., 2015. Liposomes Size Engineering by Combination of Ethanol Injection and Supercritical Processing. J. Pharm. Sci. 104 (11), 3842–3850. https://doi.org/10.1002/jps.24595.

Falco, N., Reverchon, E., Della Porta, G., 2013. Injectable PLGA/hydrocortisone formulation produced by continuous supercritical emulsion extraction. Int. J. Pharm. 441 (1-2), 589–597. https://doi.org/10.1016/j.ijpharm.2012.10.039.

Fountain, M.W., Ganjam, V.K., Schultz, R.D., 1982. LIPOSOME CARRIER VEHICLE FOR TRIIODOTHRYONINE. Clin. Exp. Pharmacol. Physiol. 9 (1), 101–105. https://doi.org/10.1111/j.1440-1681.1982.tb00784.x.

Fresta, M., Puglisi, G., 1996. Application of liposomes as potential cutaneous drug delivery systems. *in vitro* and *in vivo* investigation with radioactively labelled vesicles. J. Drug Target. 4 (2), 95–101. https://doi.org/10.3109/10611869609046267.

Gabizon, A., Papahadjopoulos, D., 1988. Liposome formulations with prolonged circulation time in blood and enhanced uptake by tumors. Proc. Natl. Acad. Sci. 85 (18), 6949–6953. https://doi.org/10.1073/pnas.85.18.6949.

Gimenez-Rota, C., Palazzo, I., Scognamiglio, M.R., Mainar, A., Reverchon, E., Della Porta, G., 2019. β-Carotene, α-tocoferol and rosmarinic acid encapsulated within PLA/PLGA microcarriers by supercritical emulsion extraction: Encapsulation efficiency, drugs shelf-life and antioxidant activity. J. Supercritical Fluids 146, 199–207. https://doi.org/10.1016/j.supflu.2019.01.019.

Grøntved, L., Waterfall, J.J., Kim, D.W., Baek, S., Sung, M.-H., Zhao, L., Park, J.W., Nielsen, R., Walker, R.L., Zhu, Y.J., Meltzer, P.S., Hager, G.L., Cheng, S., 2015. Transcriptional activation by the thyroid hormone receptor through ligand-dependent receptor recruitment and chromatin remodelling. Nat Commun 6, 7048. https://doi.org/10.1038/ncomms8048.

Hellemans, J., Mortier, G., De Paepe, A., Speleman, F., Vandesompele, J., 2007. qBase relative quantification framework and software for management and automated analysis of real-time quantitative PCR data. Genome Biol 8, R19. https://doi.org/10.1186/gb-2007-8-2-r19.

Heurtault, B., 2003. Physico-chemical stability of colloidal lipid particles. Biomaterials 24 (23), 4283–4300. https://doi.org/10.1016/S0142-9612(03)00331-4.

Honary, S., Zahir, F., 2013. Effect of Zeta Potential on the Properties of Nano-Drug Delivery Systems - A Review (Part 1). Trop. J. Pharm Res 12, 255–264. https://doi.org/10.4314/tjpr.v12i2.19.

Hong, K., Yoshimura, T., Papahadjopoulos, D., 1985. Interaction of clathrin with liposomes: pH-dependent fusion of phospholipid membranes induced by clathrin. FEBS Lett. 191, 17–23. https://doi.org/10.1016/0014-5793(85)80985-6.

Huang, Z., Yin, Z., Xu, J., Fei, Y., Heng, B.C., Jiang, X., Chen, W., Shen, W., 2021. Tendon Stem/Progenitor Cell Subpopulations and Their Implications in Tendon Biology. Front. Cell Dev. Biol. 9, 631272 https://doi.org/10.3389/fcell.2021.631272.

Immordino, M.L., Dosio, F., Cattel, L., 2006. Stealth liposomes: review of the basic science, rationale, and clinical applications, existing and potential. Int J Nanomedicine 1, 297–315.

Kashapov, R., Ibragimova, A., Pavlov, R., Gabdrakhmanov, D., Kashapova, N., Burilova, E., Zakharova, L., Sinyashin, O., 2021. Nanocarriers for Biomedicine: From Lipid Formulations to Inorganic and Hybrid Nanoparticles. IJMS 22, 7055. https://doi.org/10.3390/ijms22137055.

Kim, E.-M., Jeong, H.-J., 2021. Liposomes: Biomedical Applications. Chonnam Med J 57 (1), 27. https://doi.org/10.4068/cmj.2021.57.1.27.

Kirchner, C., Liedl, T., Kudera, S., Pellegrino, T., Muñoz Javier, A., Gaub, H.E., Stölzle, S., Fertig, N., Parak, W.J., 2005. Cytotoxicity of Colloidal CdSe and CdSe/ZnS Nanoparticles. Nano Lett. 5 (2), 331–338. https://doi.org/10.1021/nl047996m.

Kohli, A.G., Kierstead, P.H., Venditto, V.J., Walsh, C.L., Szoka, F.C., 2014. Designer lipids for drug delivery: From heads to tails. J. Control. Release 190, 274–287. https://doi.org/10.1016/j.jconrel.2014.04.047.

Lee, Y., Thompson, D.H., 2017. Stimuli-responsive liposomes for drug delivery. WIREs Nanomed Nanobiotechnol 9 (5). https://doi.org/10.1002/wnan.1450.

Li, J., Wang, X., Zhang, T., Wang, C., Huang, Z., Luo, X., Deng, Y., 2015. A review on phospholipids and their main applications in drug delivery systems. Asian J. Pharm. Sci. 10 (2), 81–98. https://doi.org/10.1016/j.ajps.2014.09.004.

Liu, Y., Castro Bravo, K.M., Liu, J., 2021. Targeted liposomal drug delivery: a nanoscience and biophysical perspective. Nanoscale Horiz. 6 (2), 78–94. https://doi.org/10.1039/D0NH00605J.

Meure, L.A., Foster, N.R., Dehghani, F., 2008. Conventional and Dense Gas Techniques for the Production of Liposomes: A Review. AAPS PharmSciTech 9, 798. https://doi.org/10.1208/s12249-008-9097-x.

Miller, A., 2003. The Problem with Cationic Liposome / Micelle-Based Non-Viral Vector Systems for Gene Therapy. CMC 10, 1195–1211. https://doi.org/10.2174/0929867033457485.

Oliva, F., Berardi, A.C., Misiti, S., Verga Falzacappa, C., Iacone, A., Maffulli, N., 2013. Thyroid hormones enhance growth and counteract apoptosis in human tenocytes isolated from rotator cuff tendons. Cell Death Dis 4, e705–e705. https://doi.org/10.1038/cddis.2013.229.

Oliva, F., Maffulli, N., Gissi, C., Veronesi, F., Calciano, L., Fini, M., Brogini, S., Gallorini, M., Antonetti Lamorgese Passeri, C., Bernardini, R., Cicconi, R., Mattei, M., Berardi, A.C., 2019. Combined ascorbic acid and T3 produce better healing compared to bone marrow mesenchymal stem cells in an Achilles tendon injury rat model: a proof of concept study. J Orthop Surg Res 14 (1). https://doi.org/10.1186/s13018-019-1098-9.

Palazzo, I., Lamparelli, E.P., Ciardulli, M.C., Scala, P., Reverchon, E., Forsyth, N., Maffulli, N., Santoro, A., Della Porta, G., 2021. Supercritical emulsion extraction fabricated PLA/PLGA micro/nano carriers for growth factor delivery: Release profiles and cytotoxicity. Int. J. Pharm. 592, 120108. https://doi.org/10.1016/j.ijpharm.2020.120108.

Pireddu, R., Pibiri, M., Valenti, D., Sinico, C., Fadda, A.M., Simbula, G., Lai, F., 2018. A novel lactoferrin-modified stealth liposome for hepatoma-delivery of triiodothyronine. Int. J. Pharm. 537 (1-2), 257–267. https://doi.org/10.1016/j.ijpharm.2017.12.048.

Samuni, A.M., Lipman, A., Barenholz, Y., 2000. Damage to liposomal lipids: protection by antioxidants and cholesterol-mediated dehydration. Chem Phys Lipids 105 (2), 121–134.

Scherphof, G.L., Kamps, J.A.A.M., 1998. Receptor versus non-receptor mediated clearance of liposomes. Adv. Drug Deliv. Rev. 32 (1-2), 81–97. https://doi.org/10.1016/S0169-409X(97)00133-6.

Sercombe, L., Veerati, T., Moheimani, F., Wu, S.Y., Sood, A.K., Hua, S., 2015. Advances and Challenges of Liposome Assisted Drug Delivery. Front. Pharmacol. 6 https://doi.org/10.3389/fphar.2015.00286.

Shah, S., Dhawan, V., Holm, R., Nagarsenker, M.S., Perrie, Y., 2020. Liposomes: Advancements and innovation in the manufacturing process. Adv. Drug Deliv. Rev. 154–155, 102–122. https://doi.org/10.1016/j.addr.2020.07.002.

Siler-marinkovic, S., Mojovic, L., Davinic, V., Bugarski, B., 1997. Liposomes as Carriers of Antimicrobial Drugs. Drug Dev. Ind. Pharm. 23 (5), 483–488. https://doi.org/10.3109/03639049709148497.

Simões, S., Filipe, A., Faneca, H., Mano, M., Penacho, N., Düzgünes, N., Pedroso de Lima, M., 2005. Cationic liposomes for gene delivery. Expert Opinion on Drug Delivery 2 (2), 237–254. https://doi.org/10.1517/17425247.2.2.237.

Siontorou, C., Nikoleli, G.-P., Nikolelis, D., Karapetis, S., 2017. Artificial Lipid Membranes: Past, Present, and Future. Membranes 7, 38. https://doi.org/10.3390/membranes7030038.

Straubinger, R.M., Hong, K., Friend, D.S., Papahadjopoulos, D., 1983. Endocytosis of liposomes and intracellular fate of encapsulated molecules: Encounter with a low pH compartment after internalization in coated vesicles. Cell 32 (4), 1069–1079. https://doi.org/10.1016/0092-8674(83)90291-X.

Ta, T., Porter, T.M., 2013. Thermosensitive liposomes for localized delivery and triggered release of chemotherapy. J. Control. Release 169 (1-2), 112–125. https://doi.org/10.1016/j.jconrel.2013.03.036.

Trucillo, P., Campardelli, R., Reverchon, E., 2020. Liposomes: From Bangham to Supercritical Fluids. Processes 8, 1022. https://doi.org/10.3390/pr8091022.

Vermorken, A.J.M., Hukkelhoven, M.W.A.C., Vermeesch-Markslag, A.M.G., Goos, C.M.A.A., Wirtz, P., Ziegenmeyer, J., 2011. The use of liposomes in the topical application of steroids. J. Pharm. Pharmacol. 36, 334–336. https://doi.org/10.1111/j.2042-7158.1984.tb04387.x.

Yu, B., Lee, R.J., Lee, L.J., 2009. Microfluidic Methods for Production of Liposomes, in: Methods in Enzymology. Elsevier, pp. 129–141. https://doi.org/10.1016/S0076-6879(09)65007-2.

Zhao, Y., Cai, F., Shen, X., Su, H., 2020. A high stable pH-temperature dual-sensitive liposome for tuning anticancer drug release. Synth. Syst. Biotechnol. 5 (2), 103–110. https://doi.org/10.1016/j.synbio.2020.05.004.